

Ball-milling synthesis of ZnO@sulphur/carbon nanotubes and Ni(OH)₂@sulphur/carbon nanotubes composites for high-performance lithium-sulphur batteries

Author

Gu, Xingxing, Tong, Chuan-jia, Wen, Bo, Liu, Li-min, Lai, Chao, Zhang, Shanqing

Published

2016

Journal Title

Electrochimica Acta

Version

Accepted Manuscript (AM)

DOI

[10.1016/j.electacta.2016.03.018](https://doi.org/10.1016/j.electacta.2016.03.018)

Rights statement

© 2016, Elsevier. Licensed under the Creative Commons Attribution-NonCommercial-NoDerivatives 4.0 International Licence, which permits unrestricted, non-commercial use, distribution and reproduction in any medium, providing that the work is properly cited.

Downloaded from

<http://hdl.handle.net/10072/99575>

Griffith Research Online

<https://research-repository.griffith.edu.au>

Ball-milling synthesis of metal oxides or hydroxides wrapping sulphur/carbon nanotubes composite for lithium-sulfur batteries

Xingxing Gu^{†a,b}, Chuan-jia Tong^{†c}, Bo Wen^c, Li-min Liu^c, Chao Lai^{*a,b}, Shanqing Zhang^b

a School of Chemistry and Chemical Engineering and Jiangsu Key Laboratory of Green Synthetic Chemistry for Functional Materials, Jiangsu Normal University, Xuzhou, Jiangsu 221116, China. E-mail: laichao@jsnu.edu.cn

b Center for Clean Environment and Energy, Environmental Futures Research Institute, Griffith School of Environment, Griffith University, Gold Coast Campus, QLD 4222, Australia.

c Beijing Computational Science Research Centre, Beijing 100084, China.

Abstract

A general wet ball-milling route is employed to prepare metal oxide or hydroxide wrapping sulfur/carbon nanotubes composite, including zinc oxides/sulphur/carbon nanotubes composite (ZnO@S/CNT) and nickel hydroxides/sulphur/carbon nanotubes composite (Ni(OH)₂@S/CNT). As the cathodes in Li-S batteries, it is found the as-prepared ZnO@S/CNT composite illustrates a superior high initial capacity of 1663 mA h g⁻¹ at a charge/discharge rate of 160 mA g⁻¹, and can still maintain at approximately 942 mA h g⁻¹ after 70 cycles. While for Ni(OH)₂@S/CNT composites, its initial capacity is also as high as 1331 mAh g⁻¹, but a poorer cycling performance is presented. When the charge/discharge current increased to 1600 mA g⁻¹, a high reversible capacity of 698 mAh g⁻¹ after 200 cycles still can be obtained for the ZnO@S/CNT composite, far better than that of Ni(OH)₂@S/CNT composites. The better cycling performance and high discharge capacity can be attributed to the strong interactions between ZnO and S_x²⁻ species, which is verified by the density functional theory (DFT) calculation result that the ZnO exhibits a higher adsorption energy for Li₂S₈ than the Ni(OH)₂.

Key words: ZnO@S/CNT composite, Ni(OH)₂@S/CNT composites, Li-S batteries, HSAB theory

1. Introduction

It is well known that the demand for high performance and long-life rechargeable batteries continue to increase[1, 2]. The specific capacity and energy density of conventional lithium ion batteries (LIBs) have been insufficient for many of the aforementioned applications, i.e. electric vehicles (EV) and hybrid electric vehicles (HEV)[1]. Therefore, to search for more efficient, higher theoretical specific capacity and energy density cathodic materials for rechargeable batteries is one of the most urgent issues in energy storage[3]. Elemental sulfur, due to its high theoretical specific capacity of 1675 mAh g⁻¹ and high theoretical energy density of 2600 Wh kg⁻¹ as well as its abundant, nontoxic and low-cost[2, 4, 5], has been considered as the most promising cathode material to replace the traditional metal oxide cathodes[2, 5].

However, there are still several issues that hinder the commercialization of the lithium-sulfur (Li-S) batteries. Firstly, the inherently poor electrical conductivity of sulfur (5×10^{-30} S cm⁻¹ at 25 °C) leads to limited utilization of active material and results in low rate capability along with a poor electrochemical reversibility[2, 6]; secondly, significant structure and volumetric changes during the charge/discharge process cause rapid capacity decay and low coulombic efficiency[1, 6]; Thirdly and most important, polysulphides readily dissolve in the organic electrolyte, shuttle to anode and then react with lithium to form insulating Li₂S₂/Li₂S during the charging process, which result in a low utilization of sulphur, rapid capacity fading, low coulombic efficiency and poor cycling performance[2, 4, 6]. Work to date, a variety of strategies including electrolyte development[7, 8], anode modifications[9,

10], and cathode synthesis, etc.[11-16], have been intensively investigated in order to address the above issues in the charge/discharge process. In particular, the strategies for hindering polysulfides dissolution and trapping polysulfides are universal recognition and welcome.

Metal oxides, as the additives or coating layer could enhance the electrochemical performances of Li-S batteries have been widely reported[1, 3-5, 7, 17-24]. And Cui's group proved that there is "Ti-S interaction" during charge/discharge process in Li-S batteries, which means the chemical adsorption of sulfur in intrinsic oxygen vacancies[2]. And due to this kind of chemical adsorption, the electrochemical performances have been improved significantly. According to the hard and soft acids and bases theory (HSAB) theory[25], Ti^{4+} is a hard acid and S_x^{2-} is a soft base. Actually the soft base is preferential to combine with the soft acid, then border acid, finally hard acid[25]. Therefore some other metal oxides/hydroxide, such as ZnO, $Ni(OH)_2$, which contain border acid metal ions should have strong chemical adsorption on polysulfides as well. And recently, both the nickel hydroxide-modified sulfur/conductive carbon black ($Ni(OH)_2@S/CCB$) composite and S/ZnO composite have been employed as the cathode materials for the Li-S battery[26, 27]. As expected, the ZnO and $Ni(OH)_2$ coating cathodes exhibit better cycle stability and higher rate discharge capacity in comparison with the bare S electrode.

In recent years, ball milling technology has been widely used for grinding various materials in industrial applications. And there are several advantages for this method to synthesize electrode materials, i.e. easy to realize large scale synthesis of homogenous electrode materials, favourable for obtaining high tap density and reproducible results, and also its economy, simplicity and so on[28]. Accordingly, it is attractive and practicable to realize large-scale synthesis of metal oxide coating sulphur-based composite cathodes via facile ball-milling route.

Based on all the discussions above, in this work, we apply the wet ball-milling method to synthesize a metal oxide@S/CNT composite (ZnO@S/CNT) and a metal hydroxide@S/CNT composite (Ni(OH)₂@S/CNT) as shown in figure 1, and employ them as the cathodes in Li-S batteries, respectively. And both the ZnO@S/CNT and Ni(OH)₂@S/CNT electrodes illustrate more stable cycling performances compared to the S/CNT electrode. More interestingly, when fixed the same coating amount of ZnO and Ni(OH)₂ as well as the same sulfur content in the composite, the ZnO@S/CNT electrode demonstrates better electrochemical performances in comparison with Ni(OH)₂@S/CNT electrode. And the mechanisms are responsible for this phenomenon has been studied.

(Figure 1 The ball-milling process for preparing the ZnO@S/CNT and Ni(OH)₂@S/CNT)

2. Experimental

2.1 Samples preparation

Sulfur/carbon nanotubes (S/CNT) composite preparation: sulfur and multi-walled carbon nanotubes (diameter: 10-20 nm, length: 5-15 μ m, \geq 95%) with a weight ratio of 3:2 or 9:11 were added in the agate tank (50 mL) and then mixed well by ball-milling. The ball-milling was performed in a planetary ball mill (QM-3SP04, Nanjing) under ambient conditions at a speed of 300 rpm for 3 h. Then the S/CNT composites with around 60 % (S/CNT-60%) and 45 % (S/CNT-45%) sulfur content were obtained respectively.

The synthesis of ZnO-coated sulfur/CNT (ZnO@S/CNT) composite: Zn(CH₃COO)₂·2H₂O (0.4 g, \geq 99.5%), ethanol (5mL) and S/CNT-60% composite (0.6 g) were added in the agate tank under stirring. When the mixture turn viscous, concentrated ammonia (1 mL, 30 wt%) were introduced, and then grinded by ball-milling for 3 h with a speed of 500 r min⁻¹. The obtained sample was washed by water and ethanol, and dried at 60 °C for 12 h.

The synthesis of Ni(OH)₂@S-CNT: same experimental procedures are employed as preparing ZnO@S/CNT except adding 0.477 g NiCl₂·6H₂O as the precursor.

2.2 Samples characterization

The as-prepared samples were characterized by X-ray diffraction (XRD, Model LabX-6000, Shimadzu, Japan), scanning electron microscopy (SEM, JSM-7001F), and transmission electron microscopy (TEM, FEI Tecnai F20). The Brunauer–Emmett–Teller (BET) method using nitrogen adsorption and desorption isotherms was performed on an ASAP 2020 system (Micromeritics, USA). Thermogravimetric analyses (TGA) are carried out under N₂ atmosphere on a Series Q500 instrument (TA Instruments, USA) to detect the accurate sulfur loadings in the S/CNT, Ni(OH)₂@S/CNT and ZnO@S/CNT composites in a temperature range from room temperature to 800 °C with increasing rate of 10 °C min⁻¹.

2.3 Electrochemical tests

The working electrodes were prepared by compressing a mixture of active materials, acetylene black, and binder (polytetrafluoroethylene, PTFE) in a weight ratio of 70:20:10. And the S mass loading in the electrodes are all around 1.35 mg/cm² according to the sulfur content in the composites. Lithium metal was used as the counter and reference electrode. The electrolyte was Lithium bis(trifluoromethanesulfonyl)imide (2.8 M) dissolved in a mixture of dimethoxyethane (DME) and dioxolane (DOL) in a volume ratio of 1:1. The LAND-CT2001A galvanostatic testers were employed to measure the electrochemical capacity at a current density of 160 and 1600 mA g⁻¹ and the cycle life of working electrodes at room temperature. The cut-off potentials for charge and discharge were set at 3.0 and 1.5 V (vs. Li⁺/Li), respectively. Electrochemical impedance spectra (EIS) were collected using solartron 1287 electrochemical workstation. A perturbation of 5 mV was applied and data collected under PC control (custom software) from 100 kHz to 10 mHz.

2.4 Computational Details

The computations were performed using the Vienna Ab Initio Simulation Package (VASP)[29-31] in the framework of density functional theory (DFT). The generalized gradient approximation (GGA) with the PBE functional was used to treat the exchange-correlation interaction between electrons[32]. Spin-polarizations were included in Ni(OH)₂ system, and the magnetic ordering was carefully considered. In addition, on-site Coulomb repulsion was utilized, and the effective U-J terms, from linear response theory[33], was 5.5 eV for transition metal element Ni. To improve the description of long-range van der Waals (vdW) interaction, we have employed the DFT-D3 method[34, 35]. The cutoff energy of the projector augmented plane-wave basis set is 500 eV to ensure an accuracy of the energy of 1 meV per atom. The full geometry optimizations are carried out with the convergence thresholds of 10⁻⁵ eV and 1×10⁻² eV/Å for total energy and ionic force, respectively. The k-point sampling uses the Monkhorst–Pack scheme on a 3×3×1 mesh.

3. Results and discussion

Figure 2a shows the XRD patterns of the S/CNT-45%, ZnO@S/CNT, and Ni(OH)₂@S/CNT composites. From the XRD spectrums, It can be observed the precursor Zn(CH₃COO)₂·2H₂O has successfully converted into the ZnO (closed diamond) with adding the ammonia during ball-milling process. And for the precursor NiCl₂·6H₂O, after ball-milling, Ni(OH)₂ (closed circle) has been successfully obtained from the precursor of NiCl₂·6H₂O. And from TGA curves as shown in Figure 2b, the sulfur content in the composites are determined to be 44.91 wt%, 58.79 wt%, 44.03 wt%, and 44.84 wt% for the S/CNT-45%, S/CNT-60%, Ni(OH)₂@S/CNT and ZnO@S/CNT composites, respectively. Accordingly, the Ni(OH)₂ and ZnO coatings contents in the composites are ca. 25.11 wt% and 23.72 wt% respectively, which keep almost the same content.

(Figure 2a XRD diffractograms of S/CNT, ZnO@S/CNT and Ni(OH)₂@S/CNT composites; Figure 2b TGA curves of S/CNT, ZnO@S/CNT and Ni(OH)₂@S/CNT composites)

The morphologies of S/CNT, ZnO@S/CNT and Ni(OH)₂@S/CNT are shown in figure 3. From the figure 3a-b, it can be observed that the CNTs have provided 3D network structure to support the sulfur. What's more this 3D network is beneficial to electrons and ions transportation during the charge/discharge process[36, 37]. While from figure 3c to figure 3f, remarkable morphologies differences from the CNT/S composite are observed, which is due to the ZnO and Ni(OH)₂ have coated on the surface of the CNT/S composite. however, there is not a distinctive morphology difference between ZnO@S/CNT and Ni(OH)₂@S/CNT composites. And as shown in table S1, ZnO@S/CNT composite and Ni(OH)₂@S/CNT composite nearly have the same BET surface areas, but both smaller than CNT/S composite, which means the ZnO and Ni(OH)₂ have been tightly coated on the S/CNT composite surface. In addition, the EDS and element mapping in Fig. S1 and S2 reveal the ZnO and Ni(OH)₂ distributed relatively homogeneously in the S/CNT frameworks.

(Figure 3 SEM images of the S/CNT (a, b), ZnO@S/CNT(c, d), Ni(OH)₂@S/CNT (e, f).)

The TEM images of ZnO@S/CNT and Ni(OH)₂@S/CNT are revealed in the figure 4. The high-resolution TEM image of ZnO@S/CNT (figure 4b) demonstrates that the crystal lattice fringes with *d*-spacing of 0.26 nm corresponds to the (002) plane of the ZnO, and the high-resolution TEM image of Ni(OH)₂@S/CNT (figure 4d) demonstrates that the crystal lattice fringes with *d*-spacing of 0.233 nm corresponds to the (101) plane of the Ni(OH)₂, which agrees well with the XRD results.

(Figure 4 TEM images of the ZnO@S/CNT (a, c), Ni(OH)₂@S/CNT (b, d).)

Typical voltage capacity profiles of ZnO@S/CNT, Ni(OH)₂@S/CNT and S/CNT-45% cathodes at the first cycle are shown in figure 5. Two typical plateaus like all the sulfur-containing electrodes can be observed for both samples, which could be assigned to a two-step reaction of sulfur with lithium during the discharge process[2, 6, 38, 39]. The initial discharge-charge capacities of the ZnO@S/CNT composite and Ni(OH)₂@S/CNT composite

are 1662.5 mAh g⁻¹ and 1313.0 mAh g⁻¹, respectively, which are both higher than that of S/CNT-45% (1058 mAh g⁻¹). Further, it should be mentioned that ZnO@S/CNT composite demonstrates a much lower polarization potential as compared to Ni(OH)₂@S/CNT composite and S/CNT-45% composite, indicating a better kinetic process.

(Figure 5 Galvanostatic charge-discharge curves of the ZnO@S/CNT, Ni(OH)₂@S/CNT and S/CNT-45% cathodes at 160 mA g⁻¹.)

Figure 6a and b illustrates the cycling performances of ZnO@S/CNT, Ni(OH)₂@S/CNT and S/CNT-45% cathodes at the current density of 160 mA g⁻¹ and 1600 mA g⁻¹, respectively. At the low discharge rate (160 mA g⁻¹), it is obvious that ZnO@S/CNT composite electrode shows excellent cycle stability after initial five cycles. For example, the discharge capacity of the 6th cycle is 988 mAh g⁻¹, and it can stably maintain at 942 mAh g⁻¹ after 70 cycles, for which the capacity retention is 95.3%. For the Ni(OH)₂@S/CNT cathodes, the discharge capacity gradually decrease, and stays at 728 mAh g⁻¹ after 70 cycles. While for S/CNT-45% cathodes, it can only remain a reversible capacity of 598 mAh g⁻¹ after 70 cycles with low capacity retention of 56.5%. When the current density is increased 10 times to 1600 mA g⁻¹, it is distinctly noticed that ZnO@S/CNT composite electrode illustrates much better cycling performance compared to Ni(OH)₂@S/CNT and S/CNT-45% composite. The initial discharge capacity is 1318.2 mAh g⁻¹, and can retain at 697.4 mAh g⁻¹ after 200 cycles for the ZnO@S/CNT composite. Following on the Ni(OH)₂@S/CNT composite owns a reversible capacity of 489.5 mAh g⁻¹ after 200 cycles at the current density of 1600 mA g⁻¹. While the S/CNT-45% composite could only remain a reversible capacity of 366 mAh g⁻¹ after 200 cycles. All the above cycling results demonstrate the ZnO and Ni(OH)₂ coating effectively promote the cycling stability of the Li-S batteries. When compared with other metal oxide-based sulfur composites cathodes as shown in table S1, our results show superiorities on the initial capacity and high rate capability.

(Figure 6 Cycle life of the ZnO@S/CNT, Ni(OH)₂@S/CNT and S/CNT-45% composite cathodes at 160 mA g⁻¹ (a) and 1600 mA g⁻¹ (b).)

Interestingly, it is demonstrated that, when fixed the same coating amount of ZnO and Ni(OH)₂ as well as the same sulfur content in the composite, the ZnO@S/CNT cathodes show better electrochemical performances compared Ni(OH)₂@S/CNT cathodes. The different electrochemical performance is likely owing to the following two factors: 1) ZnO@S/CNT composite presents a better kinetic process, which can be confirmed by the EIS results below. In addition, at high discharge rate (1600 mA g⁻¹), the capacities of the Ni(OH)₂@S/CNT electrodes has a slight increasing process from the second cycle to tenth cycle, indicating an activation process during charge/discharge process. While the ZnO@S/CNT doesn't show this phenomenon, which also suggests the ZnO@S/CNT electrode has a better contact between electrolyte and active material after cycling and thus results in a quicker kinetics[40]. 2) the soft S_x²⁻ bases prefer to being adsorbed by Zn²⁺ due to the weaker acidity compared to Ni²⁺ according to the HASB theory[25].

In order to understand why the ZnO@S/CNT electrode reveals better electrochemical performance compared to the Ni(OH)₂@S/CNT electrode, First we conducted the SEM analysis (as shown in Fig. S3) on the ZnO@S/CNT and Ni(OH)₂@S/CNT electrode after cycling X cycles, and from the SEM results, it can be observed that the integrity of the ZnO@S/CNT electrode is better than Ni(OH)₂@S/CNT, which is one possible factor to contribute the ZnO@S/CNT electrode demonstrating better cycling performances. Then the EIS of the ZnO@S/CNT and Ni(OH)₂@S/CNT electrode after initial cycle at the current density of 160 mA g⁻¹ has been investigated too. As shown in figure 7a, both the ZnO@S/CNT electrode and Ni(OH)₂@S/CNT electrode illustrate two obvious semicircles from the Nyquist plot. The semicircle in the high frequency is related to the solid-electrolyte-interface (SEI) film, and the corresponding diameter represents the resistance of the Li₂S (or

Li₂S₂) film (R_s)[6, 41]; while the semicircle in the middle frequency is attributed to the interface charge-transfer process of as-prepared nanocomposites cathode, and the corresponding diameter represents the charge-transfer resistance (R_{ct})[6, 19, 42]. In addition, the intercept at the real axis Z' corresponds to the combined resistance (R_e), which is determined by the ionic resistance of the electrolyte, the intrinsic resistance of the active materials, and the contact resistance at the metal oxide/hydroxide@CNT/S nanocomposites/current collector interface[42]. The fitted R_e , R_s , R_{ct} values of the cells according to the equivalent circuit (figure 7b) are shown in table 1. It can be observed that the R_e value of ZnO@S/CNT is smaller than that of Ni(OH)₂@S/CNT, which is due to the better contact between the active materials and the electrolyte, corresponding the higher ionic conductivity and lower contact resistance[6]. Same as the R_s , the ZnO@S/CNT illustrates smaller values, which indicates thinner solid-electrolyte-interface (SEI) film that originated from the Li₂S₂/Li₂S film growing on the surface of the electrode[6, 38]. In another words, the ZnO can more efficiently prevent the polysulfides from shuttling to the anode[39]. More importantly, the R_{ct} values of ZnO@S/CNT electrode is far smaller than that of Ni(OH)₂@S/CNT electrode, indicating the higher conductivity of the ZnO@S/CNT composite[6, 38, 39]. The smaller R_{ct} value corresponds to the quicker kinetics and higher utilization efficiency of the active materials. Therefore, according the above advantages of the ZnO@S/CNT electrode, it should reveal better electrochemical performances.

(Figure 7 The Nyquist plots of the Li–S cells after initial cycle at the current density of 160 mA g⁻¹ (a) and the corresponding equivalent circuit models (b).)

(Table 1 Impedance parameters calculated according to the equivalent circuits.)

What's more, the DFT calculations are applied to further explain why the ZnO can more efficiently to prevent the polysulfides shuttling compared to the Ni(OH)₂ and thus the ZnO@S/CNT composite demonstrates better cycling performances. Since low index (100)

surface is the most stable face of ZnO[43] and hexagonal Ni(OH)₂ is a multi-layer stacking material[44-46], then to simplify the calculation, we employed a three-layer thickness (100) surface of ZnO and monolayer of Ni(OH)₂ as the modeling substrate, and Li₂S₈ as the models for the lithium polysulfide species. The corresponding optimized adsorption configurations are shown in figure 8a. Compared with Ni(OH)₂, the (100) surface of ZnO has larger polarization and more active sites. Although the adding H atoms can passivate the exposed O atoms to determine the stability of the surface, the remaining exposed Zn atoms can still bond with S atoms in Li₂S₈, which agrees well with the HASB theory that the S_x²⁻ species are easier adsorbed by the Zn²⁺. As a result, ZnO exhibits a very high adsorption energy (5.67 eV). As for Ni(OH)₂, since its surface is saturated with hydrogens, it will have a weak interaction with Li₂S₈. But from the Bode's diagram[47], it can be seen that Ni(OH)₂ can easily transform into NiOOH by losing half of H atoms. Therefore we adopted a reliable H vacancy here with its concentration of only 3.1% as shown in figure 8b. Then the new exposed atom O, as an active adsorption site, can strongly bond with Li₂S₈. Even so, finally the calculated adsorption energy (2.43 eV by PBE and 2.39 eV by PBE+U) indicates that ZnO affords a much stronger adsorption of polysulfides than that of Ni(OH)₂ due to its polarized and active surface characteristic. It is reasonable to conclude that the higher adsorption energy on lithium polysulfides contributes to the high cycle stability.

(Figure 8 The most preferential adsorption structures of Li₂S₈ on ZnO (a) and Ni(OH)₂ (b).

All the models are shown in the most stable configuration.)

4. Conclusions

The ZnO@S/CNT and Ni(OH)₂@S/CNT composites have been successfully prepared via the ball milling process and applied as the cathode materials for Li-S batteries. By coating ZnO and Ni(OH)₂ on the surface of S/CNT composites, the cycling performances have improved significantly, and high reversible capacity can be obtained, showing obvious

advantages over bare S/CNT composites. For ZnO@S/CNT composite, a high reversible discharge capacity of 941.6 mAh g⁻¹ can be obtained after 70 cycles at the current density of 160 mA g⁻¹, and it can stably retain at 697.4 mAh g⁻¹ after 200 cycles when the current density increased to 1600 mA g⁻¹. Most importantly, the HSAB theory has been proposed to explain why the ZnO as the additive or coating can more effectively improve the cycling performance in Li-S batteries compared to the Ni(OH)₂, and this hypothesis is supported by the DFT calculation results, for which ZnO displays stronger binding ability on the polysulfides compared to that of Ni(OH)₂. Additionally, the wet ball-milling route can be applied to realize large-scale synthesis of various metal oxide-sulfur composites as the cathodes for acquiring high-performance Li-S batteries.

Acknowledgements

Xingxing Gu and Chuan-jia Tong has contributed equally to this work. And this work has been supported by the Chinese National Science Funds (No. 51202094); the Priority Academic Program Development of Jiangsu Higher Education Institutions; and the ARC Discovery Grants from the Australian Research Council is also acknowledged. And the authors also want to thank Yang Chen for his kind help on drawing the synthesis schematic.

References:

- [1] Z. W. Seh, W. Li, J.J. Cha, G. Zheng, Y. Yang, M.T. McDowell, P.C. Hsu, Y. Cui, Sulphur-TiO₂ yolk-shell nanoarchitecture with internal void space for long-cycle lithium-sulphur batteries, *Nat. Commun.*, 4 (2013) 1331-1336.
- [2] L. Zhang, L. Ji, P.A. Glans, Y. Zhang, J. Zhu, J. Guo, Electronic structure and chemical bonding of a graphene oxide-sulfur nanocomposite for use in superior performance lithium-sulfur cells, *Phys. Chem. Chem. Phys.*, 14 (2012) 13670-13675.
- [3] Y. Zhang, X. Wu, H. Feng, L. Wang, A. Zhang, T. Xia, H. Dong, Effect of nanosized Mg_{0.8}Cu_{0.2}O on electrochemical properties of Li/S rechargeable batteries, *Internat. J. Hydrogen Energy*, 34 (2009) 1556-1559.
- [4] K. Dong, S. Wang, H. Zhang, J. Wu, Preparation and electrochemical performance of sulfur-alumina cathode material for lithium-sulfur batteries, *Mater. Res. Bull.*, 48 (2013) 2079-2083.

- [5] F. Sun, J. Wang, D. Long, W. Qiao, L. Ling, C. Lv, R. Cai, A high-rate lithium–sulfur battery assisted by nitrogen-enriched mesoporous carbons decorated with ultrafine La_2O_3 nanoparticles, *J. Mater. Chem. A*, 1 (2013) 13283-13289.
- [6] X. Gu, Y. Wang, C. Lai, J. Qiu, S. Li, Y. Hou, W. Martens, N. Mahmood, S. Zhang, Microporous bamboo biochar for lithium-sulfur batteries, *Nano Res.*, 8 (2015) 129-139.
- [7] K. Jeddi, K. Sarikhani, N.T. Qazvini, P. Chen, Stabilizing lithium/sulfur batteries by a composite polymer electrolyte containing mesoporous silica particles, *J. Power Sources*, 245 (2014) 656–662.
- [8] J. Wang, S.Y. Chew, Z.W. Zhao, S. Ashraf, D. Wexler, J. Chen, S.H. Ng, S.L. Chou, H.K. Liu, Sulfur–mesoporous carbon composites in conjunction with a novel ionic liquid electrolyte for lithium rechargeable batteries, *Carbon*, 46 (2008) 229-235.
- [9] Y.M. Lee, N.-S. Choi, J.H. Park, J.-K. Park, Electrochemical performance of lithium/sulfur batteries with protected Li anodes, *J. Power Sources*, 119-121 (2003) 964–972.
- [10] J.H. Lee, H.Y. Lee, S.M. Oh, S.J. Lee, K.Y. Lee, S.M. Lee, Effect of carbon coating on electrochemical performance of hard carbons as anode materials for lithium-ion batteries, *J. Power Sources*, 166 (2007) 250–254.
- [11] L. Yin, J. Wang, F. Lin, J. Yang, Y. Nuli, Polyacrylonitrile/graphene composite as a precursor to a sulfur-based cathode material for high-rate rechargeable Li–S batteries, *Energy Environ. Sci.*, 5 (2012) 6966–6972.
- [12] X. Ji, K.T. Lee, L.F. Nazar, A highly ordered nanostructured carbon-sulphur cathode for lithium-sulphur batteries, *Nat. Mater.*, 8 (2009) 500–506.
- [13] G.L. Xu, Y.F. Xu, J.C. Fang, X.X. Peng, F. Fu, L. Huang, J.T. Li, S.G. Sun, Porous graphitic carbon loading ultra high sulfur as high-performance cathode of rechargeable lithium-sulfur batteries, *ACS Appl. Mater. Interf.*, 5 (2013) 10782–10793.
- [14] G. He, S. Evers, X. Liang, M. Cuisinier, A. Garsuch, L.F. Nazar, Tailoring porosity in carbon nanospheres for lithium-sulfur battery cathodes, *ACS NANO*, 7 (2013) 10920–10930.
- [15] J.-Q. Huang, Q. Zhang, S.-M. Zhang, X.-F. Liu, W. Zhu, W.-Z. Qian, F. Wei, Aligned sulfur-coated carbon nanotubes with a polyethylene glycol barrier at one end for use as a high efficiency sulfur cathode, *Carbon*, 58 (2013) 99-106.
- [16] L. Yu, N. Brun, K. Sakaushi, J. Eckert, M.M. Titirici, Hydrothermal nanocasting: Synthesis of hierarchically porous carbon monoliths and their application in lithium–sulfur batteries, *Carbon*, 61 (2013) 245-253.
- [17] B. Ding, L. Shen, G. Xu, P. Nie, X. Zhang, Encapsulating sulfur into mesoporous TiO_2 host as a high performance cathode for lithium–sulfur battery, *Electrochim. Acta*, 107 (2013) 78-84.
- [18] C.S. Kim, A. Guerfi, P. Hovington, J. Trottier, C. Gagnon, F. Barray, A. Vijh, M. Armand, K. Zaghbi, Facile dry synthesis of sulfur- LiFePO_4 core–shell composite for the scalable fabrication of lithium/sulfur batteries, *Electrochem. Commun.*, 32 (2013) 35-38.
- [19] Q. Li, Z. Zhang, K. Zhang, L. Xu, J. Fang, Y. Lai, J. Li, Synthesis and electrochemical performance of TiO_2 –sulfur composite cathode materials for lithium–sulfur batteries, *J. Solid State Electrochem.*, 17 (2013) 2959–2965.

- [20] X. Tao, J. Wang, Z. Ying, Q. Cai, G. Zheng, Y. Gan, H. Huang, Y. Xia, C. Liang, W. Zhang, Y. Cui, Strong sulfur binding with conducting Magneli-phase $Ti_{(n)}O_{2(n-1)}$ nanomaterials for improving lithium-sulfur batteries, *Nano Lett.*, 14 (2014) 5288-5294.
- [21] Z. Liang, G. Zheng, W. Li, Z. W. Seh, H. Yao, K. Yan, D. Kong, Y. Cui, Sulfur cathodes with hydrogen reduced titanium dioxide inverse opal structure, *ACS NANO*, (2014).
- [22] K.T. Lee, R. Black, T. Yim, X. Ji, L.F. Nazar, Surface-initiated growth of thin oxide coatings for Li-sulfur battery cathodes, *Adv. Energy Mater.*, 2 (2012) 1490-1496.
- [23] Y. Zhang, Y. Zhao, A. Yermukhambetova, Z. Bakenov, P. Chen, Ternary sulfur/polyacrylonitrile/ $Mg_{0.6}Ni_{0.4}O$ composite cathodes for high performance lithium/sulfur batteries, *J. Mater. Chem. A*, 1 (2013) 295-301.
- [24] M. Yu, W. Yuan, C. Li, J.-D. Hong, G. Shi, Performance enhancement of a graphene-sulfur composite as a lithium-sulfur battery electrode by coating with an ultrathin Al_2O_3 film via atomic layer deposition, *J. Mater. Chem. A*, 2 (2014) 7360-7366.
- [25] R.G. Pears, Hard and soft acids and bases, *J. Am. Chem. Soc.*, 85 (1963) 3533-3539.
- [26] X. Liang, Q. Song, Y. Liu, H. Liu, Preparation of ZnO porous nanostructures and its application in cathode material for lithium sulfur battery, *Int. J. Electrochem. Sci.*, 10 (2015) 9333-9341.
- [27] X.-Q. Niu, X.-L. Wang, D. Xie, D.-H. Wang, Y.-D. Zhang, Y. Li, T. Yu, J.-P. Tu, Nickel hydroxide-modified sulfur/carbon composite as a high-performance cathode material for lithium sulfur battery, *ACS Appl. Mater. Interf.*, 7 (2015) 16715-16722.
- [28] G. Liu, Z. Su, D. He, C. Lai, Wet ball-milling synthesis of high performance sulfur-based composite cathodes: The influences of solvents and ball-milling speed, *Electrochim. Acta*, 149 (2014) 136-143.
- [29] G. Kresse, Efficient iterative schemes for ab initio total-energy calculations using a plane-wave basis set, *Phys. Rev. B*, 54 (1996) 11169-11186.
- [30] P.E. Blochl, Projector augmented-wave method, *Phys. Rev. B*, 50 (1994) 17953-17979.
- [31] G. Kresse, From ultrasoft pseudopotentials to the projector augmented-wave method, *Phys. Rev. B*, 59 (1999) 1758-1775.
- [32] J.P. Perdew, K. Burke, M. Ernzerhof, Generalized gradient approximation made simple, *Phys. Rev. Lett.*, 77 (1996) 3865-3868.
- [33] M. Cococcioni, S. de Gironcoli, Linear response approach to the calculation of the effective interaction parameters in the LDA+U method, *Phys. Rev. B*, 71 (2005) 035105-1-035105-16.
- [34] S. Grimme, S. Ehrlich, L. Goerigk, Effect of the damping function in dispersion corrected density functional theory, *J. Comput. Chem.*, 32 (2011) 1456-1465.
- [35] S. Grimme, J. Antony, S. Ehrlich, H. Krieg, A consistent and accurate ab initio parametrization of density functional dispersion correction (DFT-D) for the 94 elements H-Pu, *J. Chem. Phys.*, 132 (2010) 154104-1-154104-19.
- [36] Y.S. Su, A. Manthiram, A new approach to improve cycle performance of rechargeable lithium-sulfur batteries by inserting a free-standing MWCNT interlayer, *Chem. Commun.*, 48 (2012) 8817-8819.

- [37] J.X. Song, Z.X. Yu, T. Xu, S.R. Chen, H. Sohn, M. Regula, D.H. Wang, Flexible freestanding sandwich-structured sulfur cathode with superior performance for lithium-sulfur batteries, *J. Mater. Chem. A*, 2 (2014) 8623-8627.
- [38] X. Gu, C. Lai, F. Liu, W. Yang, Y. Hou, S. Zhang, A conductive interwoven bamboo carbon fiber membrane for Li-S batteries, *J. Mater. Chem. A*, 3 (2015) 9502-9509.
- [39] X. Gu, C.-J. Tong, C. Lai, J. Qiu, X. Huang, W. Yang, B. Wen, L.-M. Liu, Y. Hou, S. Zhang, Porous nitrogen and phosphorous dual doped graphene blocking layer for high performance Li-S batteries, *J. Mater. Chem. A*, 3 (2015) 16670-16678.
- [40] Y. Zhang, Y. Zhao, Z. Bakenov, A simple approach to synthesize nanosized sulfur/graphene oxide materials for high-performance lithium/sulfur batteries, *Ionics*, 20 (2014) 1047-1050.
- [41] J. Zhu, D. Wang, L. Wang, X. Lang, W. You, Facile synthesis of sulfur coated SnO₂-graphene nanocomposites for enhanced lithium ion storage, *Electrochim. Acta*, 91 (2013) 323-329.
- [42] B. Ding, C. Yuan, L. Shen, G. Xu, P. Nie, X. Zhang, Encapsulating sulfur into hierarchically ordered porous carbon as a high-performance cathode for lithium-sulfur batteries, *Chem. Eur. J.*, 19 (2013) 1013-1019.
- [43] B. Meyer, D. Marx, Density-functional study of the structure and stability of ZnO surfaces, *Phys. Rev. B*, 67 (2003) 035403-1-035403-11.
- [44] K. Watanabe, T. Kikuoka, N. Kumagai, Physical and electrochemical characteristics of nickel hydroxide as a positive material for rechargeable alkaline batteries, *J. Appl. Electrochem.*, 25 (1995) 219-226.
- [45] D.E. Reisner, A.J. Salkind, P.R. Strutt, T.D. Xiao, Nickel hydroxide and other nanophase cathode materials for rechargeable batteries, *J. Power Sources*, 65 (1997) 231-233.
- [46] Z.-K. Tang, W.-W. Liu, D.-Y. Zhang, W.-M. Lau, L.-M. Liu, Tunable band gap and magnetism of the two-dimensional nickel hydroxide, *RSC Adv.*, 5 (2015) 77154-77158.
- [47] H. Bode, K. Dehmelt, J. Witte, Zur kenntnis der nickelhydroxidelektrode—I.Über das nickel (II)-hydroxidhydrat, *Electrochim. Acta*, 11 (1966) 1079-1087.

Figure Captions

Figure 1 The ball-milling process for preparing the ZnO@S/CNT and Ni(OH)₂@S/CNT

Figure 2 XRD diffractograms of S/CNT, ZnO@S/CNT and Ni(OH)₂@S/CNT composites (a) and TGA curves of S/CNT, ZnO@S/CNT and Ni(OH)₂@S/CNT composites (b).

Figure 3 SEM images of the S/CNT (a, b), ZnO@S/CNT(c, d), Ni(OH)₂@S/CNT (e, f).

Figure 4 TEM images of the ZnO@S/CNT (a, c), Ni(OH)₂@S/CNT (b, d).

Figure 5 Galvanostatic charge-discharge curves of the ZnO@S/CNT, Ni(OH)₂@S/CNT and S/CNT-45% cathodes at 160 mA g⁻¹.

Figure 6 Cycle life of the ZnO@S/CNT, Ni(OH)₂@S/CNT and S/CNT-45% composite cathodes at 160 mA g⁻¹ (a) and 1600 mA g⁻¹ (b).

Figure 7 The Nyquist plots after 100 cycles of the Li-S cells (a) and the corresponding equivalent circuit models (b).

Figure 8 The most preferential adsorption structures of Li₂S₈ on ZnO (a) and Ni(OH)₂ (b). All the models are shown in the most stable configuration.

Table Captions

Table 1 Impedance parameters calculated according to the equivalent circuits.

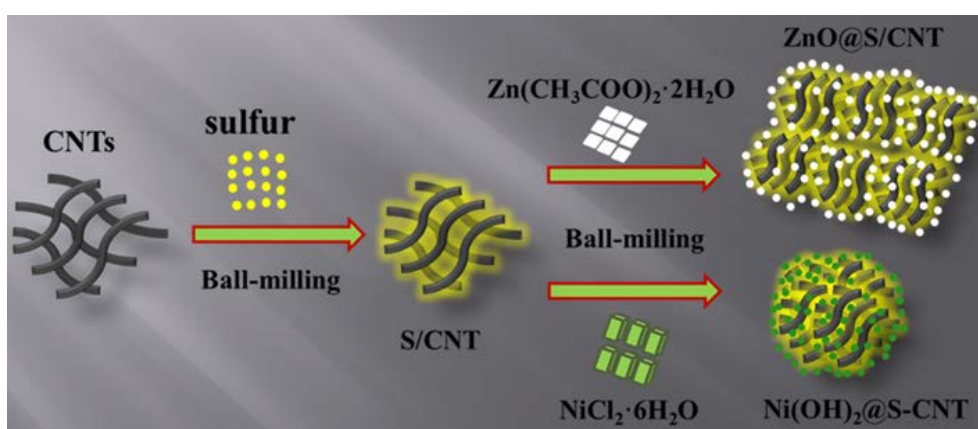


Figure 1

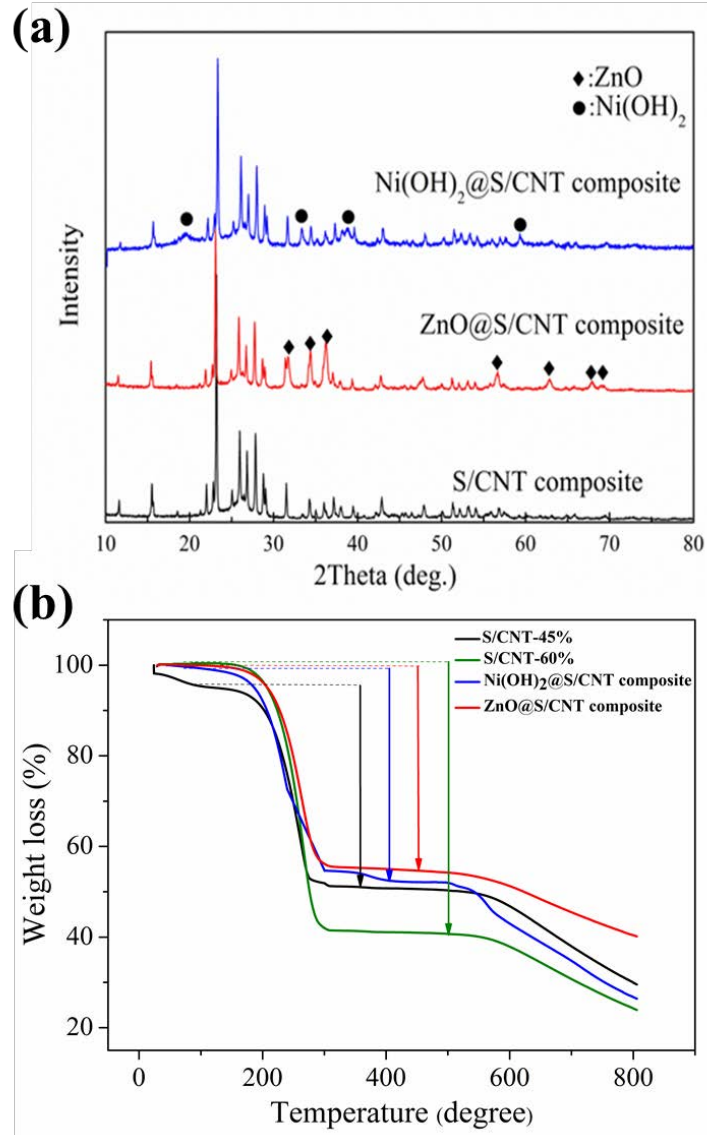


Figure 2

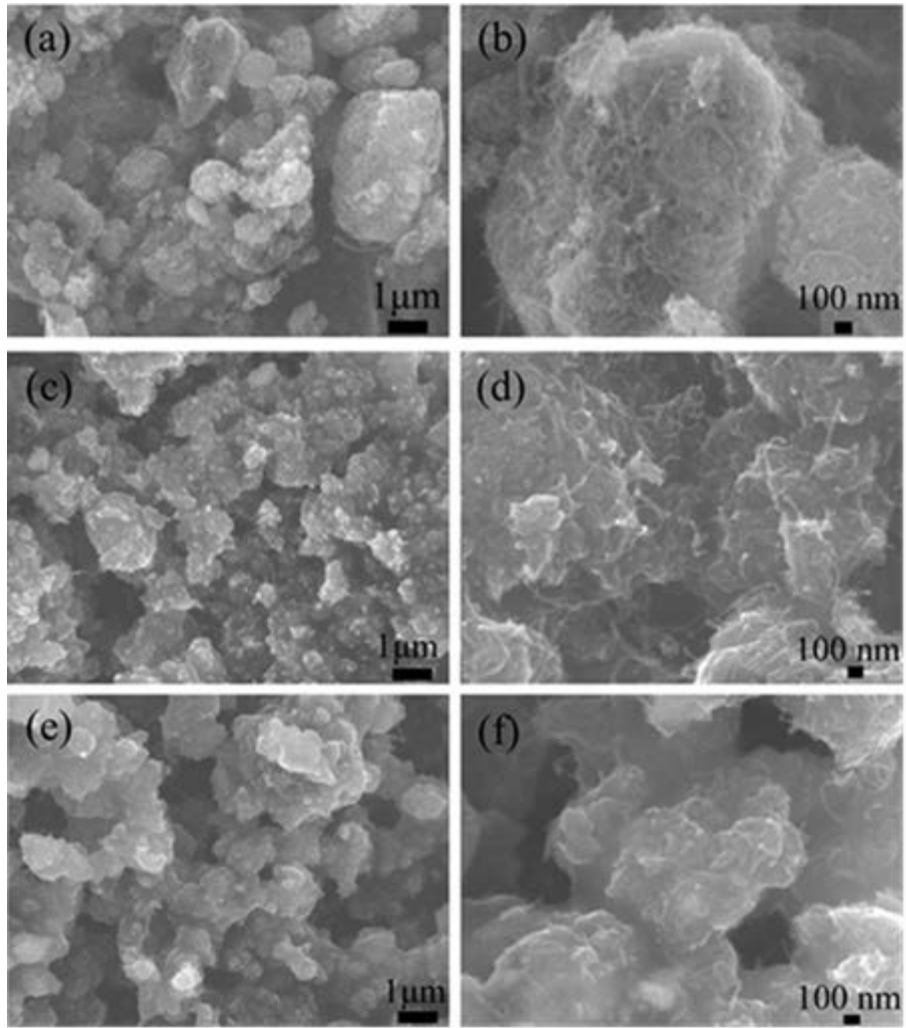


Figure 3

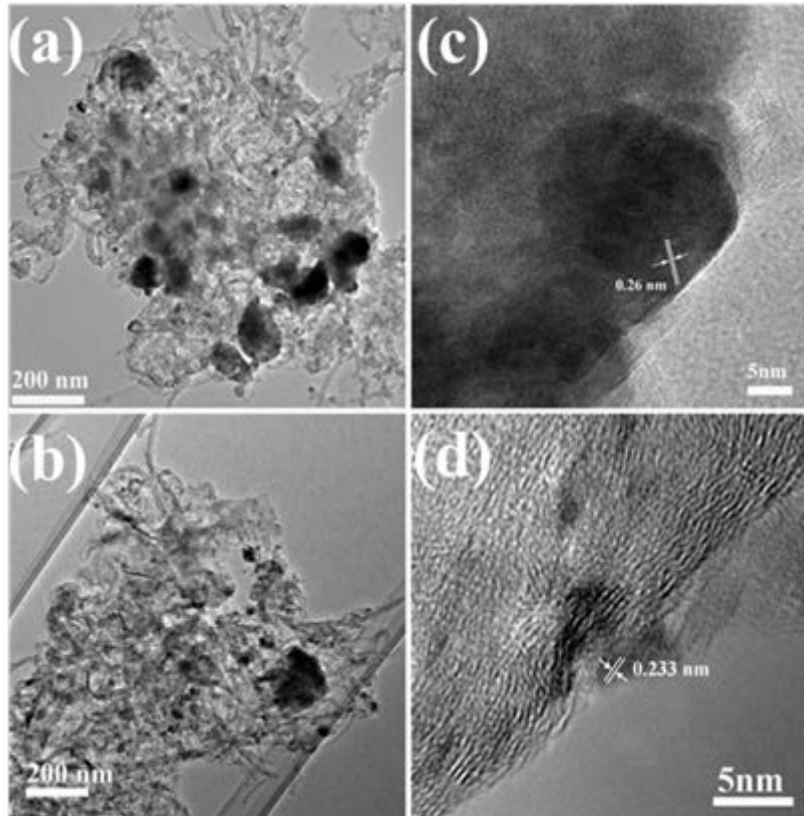


Figure 4

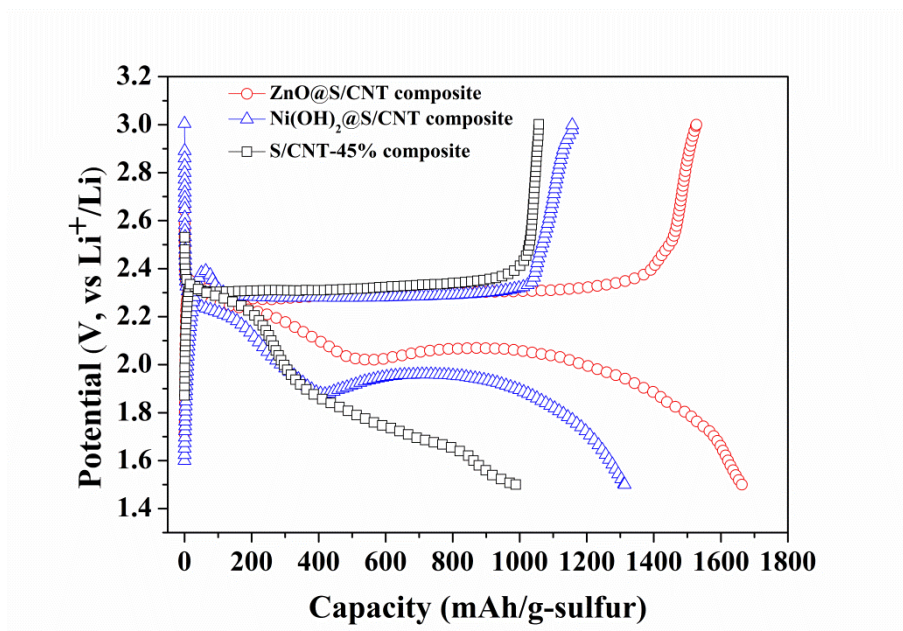


Figure 5

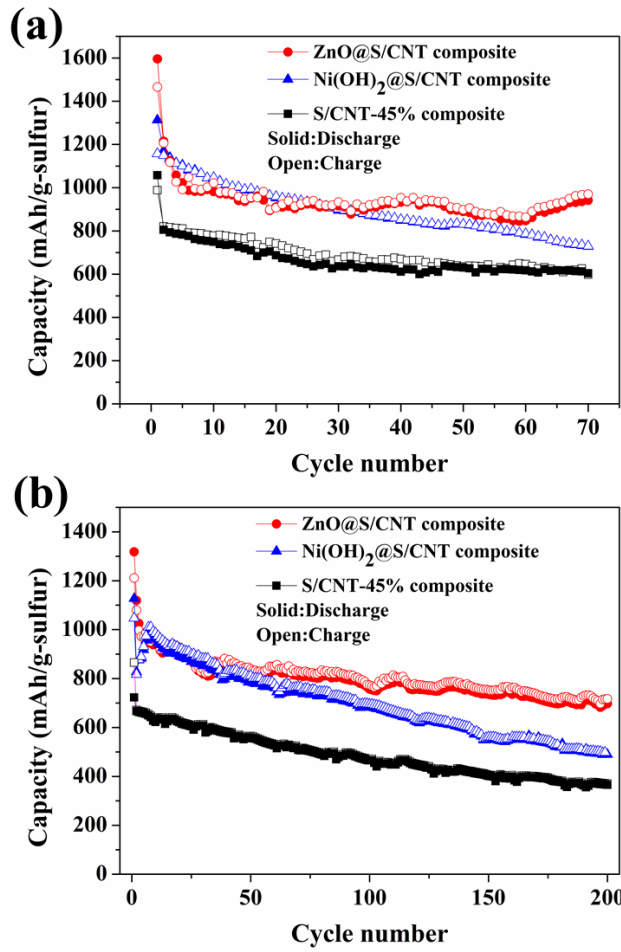


Figure 6

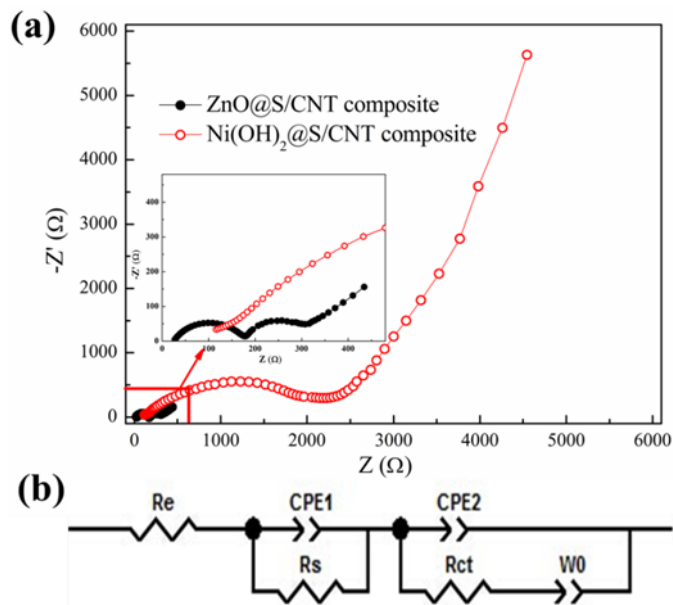


Figure 7

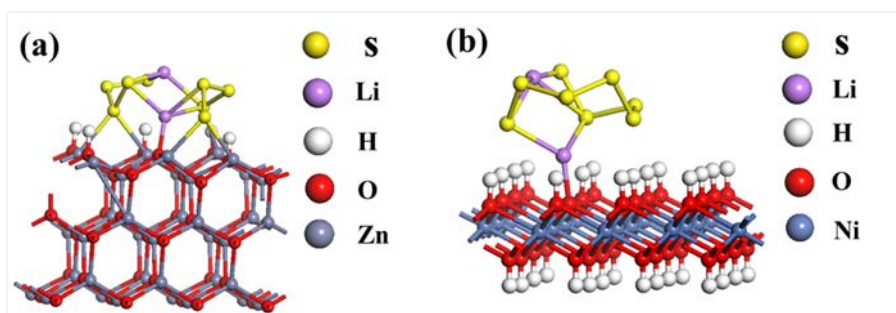


Figure 8

Table 1

Sample name	Cycle number	Resistance		
		R_e (Ω)	R_s (Ω)	R_{ct} (Ω)
ZnO@S/CNT	1 th cycles	26.03	155.7	104
Ni(OH) ₂ @S/CNT	1 th cycles	103.2	264.5	2136